Dielectrophoretic assembly of insulinoma cells and fluorescent nanosensors into three-dimensional 'pseudo-islet' constructs

R. Pethig, A. Menachery, E. Heart, R.H. Sanger and P.J.S. Smith

Abstract: Dielectrophoretic forces, generated by radio-frequency voltages applied to micromachined, transparent, indium tin oxide electrodes, have been used to condense suspensions of insulinoma cells (BETA-TC-6 and INS-1) into a 10x10 array of three-dimensional cell constructs. Some of these constructs, measuring approximately 150 μm in diameter and 120 μm in height, and containing around 1000 cells, were of the same size and cell density as a typical islet of Langerhans. With the dielectrophoretic force maintained, these engineered cell constructs were able to withstand mechanical shock and fluid flow forces. Reproducibility of the process required knowledge of cellular dielectric properties, in terms of membrane capacitance and membrane conductance, which were obtained by electrorotation measurements. The ability to incorporate fluorescent nanosensors, as probes of cellular oxygen and pH levels, into these 'pseudo-islets' was also demonstrated. The footprint of the 10x10 array of cell constructs was compatible with that of a 1536 microtitre plate, and thus amenable to optical interrogation using automated plate reading equipment.

R. Pethig, A. Menachery, E. Heart, R.H. Sanger and P.J.S. Smith are with the BioCurrents Research Centre, Program in Molecular Physiology, Marine Biological Laboratory, Woods Hole, MA 02543, USA

R. Pethig and A. Menachery are also with the School of Electronic Engineering, University of Wales, Bangor, Gwynedd, LL57 1UT, UK

1. Introduction:

This work is directed towards studying the electrophysiological properties of insulin-secreting cells (BETA-TC-6 and INS-1 insulinoma cells) as they transform from a monolayer cell culture to a three-dimensional construct that mimics localized structures (known as islets of Langerhans) that exist within the pancreas. We are extending the capabilities of electrochemical sensors and probes already developed in our laboratory [e.g., 1-3] and, as described here, the method chosen to construct the three-dimensional 'pseudo-islets' is the electrokinetic technique known as dielectrophoresis (DEP) [4]. The long-term objective is to use these artificial cell structures to study cell-cell communication through junctional complexes and to understand how this controls the synchronous functioning of islets. We hope this will lead to new cell-based assays for drugs, or the engineering of islet implants, to alleviate diabetes.

Most *in vitro* studies of the electrophysiological properties of cells have employed either monolayer cell cultures or thin tissue slices. Cells in culture adhere to their neighbors and the substrate by means of adhesion complexes, also known as tight junctions, composed of transmembrane components connected to cytoplasmic proteins and the cytoskeleton. It is now thought that these complexes not only mediate adhesion but are also engaged in the transmission of signals from the plasma membrane to the nucleus to regulate cell proliferation and differentiation. A second type of physical association between cells, the gap junction, forms a low resistance pathway allowing direct communication from one cytosolic compartment to another, transmitting both electrical and chemical information. These complexes have been proposed to be critical in coordinating the secretory activity of the islets of Langerhans [5, 6]. Furthermore, there are reported differences in the composition of cell-

cell junctional complexes for cells forming three-dimensional, compared to those forming two-dimensional (monolayer), assemblies [7].

This lack of a three-dimensional attribute, as well as the cues that result from the physico-chemical properties of a normal *in-vivo* extracellular matrix, are known to alter cell-cell signaling events of tumor cells, stem cells and differentiated cells [8-10], as well as gene expression [7]. We hope to find evidence for self-organizing processes within three-dimensional assemblies of insulin secreting cells through, for example, detection of synchronous electrical activity, calcium fluxes and insulin release. *In vitro* self-organisation of cells in an artificial three-dimensional construct has recently been described for spheroids composed of hen embryo neurons [11]. These spheroids were cultured using cells derived from hen embryo neuroepithelial tissue. The neuronal networks in these artificial spheroids behaved significantly differently from monolayer cultures, even to the extent that single spontaneous action potentials were recorded.

The pseudo-islet cell assemblies described here were produced using DEP forces generated by electrodes formed of micromachined indium tin oxide (ITO)-coated glass slides. ITO-based microelectrodes have previously been used to demonstrate selective DEP positioning of cells in a three-dimensional matrix array [12]. More recently they have been used to produce multilayer aggregates of bacteria and mammalian cells [13, 14] as well as hydrogel-encapsulated clusters of chondrocyte patterns [15]. These earlier examples used photolithography to pattern the electrodes, but here we have employed laser micromachining [14] to fabricate an array of 200 μm diameter holes in the conducting ITO-layer. On application of an AC voltage signal the holes distort the field between the two ITO-electrodes to generate the high field gradients required to produce DEP. As shown here, this simple

electrode geometry is capable of manipulating cells by both positive and negative DEP. Negative DEP was used to condense a suspended mixture of cells and fluorescent nanosensors into an array of three-dimensional cell constructs. The nanosensors took the form of oxygen and pH sensitive dyes encapsulated inside inert nanoparticles known as PEBBLEs (probes encapsulated by biologically localized embedding) [17,18]. These engineered cell assemblies were found to be sufficiently robust to withstand mechanical shock and laminar fluid flow forces. The controlled DEP manipulation of the BETA-TC-6 and INS-1 cells required knowledge of their dielectric properties, in terms of membrane capacitance and conductance. These parameters were obtained by electrorotation measurements, and the results obtained are also reported here.

2. Experimental

2.1 Cell Samples

INS-1 and BETA-TC-6 (rat and mouse insulinoma β-cells, obtained from ATCC, Manassas, VA) were cultured using standard procedures [19] summarized here. The cells were grown in RPMI 1640 medium (Invitrogen) supplemented with 11 mM glucose, 10 mM HEPES, 10% heat-inactivated fetal calf serum, 2 mM L-glutamine, 1 mM sodium pyruvate, 50 μM β-mercaptoethanol, and 100U/ml penicillin–streptomycin. A humidified incubator was used and maintained at 37^{o}C with 5% CO_2, 95% air. Immediately before the experiments, the cells were dislodged from the culture vessels by trypsinization, and washed twice in the media to be used in the DEP and electrorotation measurements (see below).

2.2 Cell–suspending media

Cell suspending solutions of physiological osmolarity were prepared for electrorotation and DEP experiments. Solutions of three different conductivities were prepared for the electrorotation studies. A solution of conductivity 11.8 mSm^{-1} contained 2mM glucose, 5.5

mM Hepes buffer, and was adjusted to 300 mos by adding 96 gL^{-1} sucrose. The pH was adjusted to pH 7.4 using NaOH, and the final conductivity was obtained by adding 0.1M KCl. For the other preparations a stock solution was prepared, comprising: 140 mM NaCl; 5.4 mM KCl; 2.5 mM $CaCl_2$; 0.5 mM $MgCl_2$; 11 mM glucose and 5.5 mM Hepes buffer. A solution of conductivity 104 mSm^{-1} was prepared by adding 8 mL of this stock solution to 92 mL double-distilled water, plus 8.47g sucrose to give 300 mos. A 55 mSm^{-1} solution was prepared by doubling the dilution of the stock solution and adding 10.39 gL^{-1} sucrose to balance the osmolarity. The conductivities were measured at 22 (± 0.5) ^{o}C, to within ± 0.25%, using a YSI 3200 Conductivity Instrument (probe constant K = 1.0/cm).

2.3 Fluorescent nanosensors

Our objective is to monitor the electrophysiological properties of insulin-secreting cells (primary β-cells, as well as BETA-TC-6 and INS-1 insulinoma cells) in real-time, as they are formed into three-dimensional constructs using the DEP procedure described here. A potentially promising method for minimally invasive intracellular monitoring of key biological components (e.g., potassium, oxygen, calcium and pH) would be to incorporate nanosensors, rather than free dyes, directly into our artificial constructs at the time of their formation. To this end, we investigated the use of fluorescent nanosensors termed PEBBLEs (Probes Encapsulated By Biologically Localized Embedding') [17, 18]. These sensors, based on polyacrylamide, cross-linked decyl methacrylate, and silica-based sol-gel nanoparticle fabrication technologies, have been characterized in aqueous solution and also tested in intracellular surroundings. Each matrix can be used to encapsulate specific dyes, ionophores, or enzymes to produce spherical sensors of the order 100 nm in diameter. Following proven

protocols [17, 18], we prepared an acrylamide-based nanosensor to monitor extracellular pH, and another based on sol-gel encapsulation of an oxygen-sensitive platinum porphyrin dye.

In the experiments to incorporate these nanosensors into the DEP-assembled cell aggregations, $2mgml^{-1}$ of filtered, washed and air-dried PEBBLEs [18] were added to the cell suspensions before admission into the DEP chamber. The glucose concentration in the suspending medium was increased to 10 mM, by adding 0.18gm glucose plus 97ml double-distilled water to 3ml of the electrorotation stock solution, and adjusting the osmolarity to 300 mos by adding 92.2 gmL^{-1} sucrose. The conductivity of this medium was 51.5 mSm^{-1}.

2.4 Electrorotation and dielectrophoresis (DEP) experiments

Before attempting to manipulate the insulinoma cells into three-dimensional constructs by DEP, knowledge of their electrokinetic behavior in electrolytes of known conductivity was required. In particular, it was important to predict the experimental conditions required to generate either positive or negative DEP movement of the cells. This information was derived using a contact-free method known as electrorotation, and was performed as described in previous work on INS-1 cells [20]. In brief, the suspended cells (~$2x10^5$ cells/ml) were subjected to a rotating electric field, and their electrorotation responses were visualized using a Zeiss Axioskop and recorded at 30 frames/sec for later analysis on a TV monitor. The diameter of the cells could be determined to an accuracy of ± 0.3 μm.

The DEP chamber is shown in Fig.1, and comprised two microscope slides, located one above the other, spaced 220μm apart and encased in poly-dimethylsiloxane (PDMS). The cell suspensions were pipetted into the upper slide through one or more 1 mm diameter fluidic ports. The cells were more dense (specific gravity ~1.07 kg/l) than that of the suspending

electrolyte (~1.04 kg/l), and were observed to settle within ~5 minutes to the bottom of the chamber. To avoid the cells sinking to the bottom of the chamber before they were subjected to a DEP force, the electrodes were electrically energized either at the same time as injection of the cells into the chamber, or within 10 secs after their injection. Typically, the DEP-induced aggregations (e.g., Fig.5) were formed in less than 30 secs. The inner surfaces of the slides were coated with electrodes of indium tin oxide (ITO) of thickness ~110nm and specific resistance ~10Ω/sq. The continuity of the ITO layer of the top slide was disrupted by a 10x10 array of holes. Each hole, of diameter 200μm and spaced 600μm apart, was fabricated by machining away the ITO layer, down to the glass substrate, using a pulsed excimer laser technique [16]. These holes created repeated patterns of electric field non-uniformities in what otherwise would have been a uniform field between the capacitor-like plates of the DEP chamber. Cells located in a region of field non-uniformity will experience a DEP force of magnitude proportional to the product of the local field and the field gradient. The imposed electric field induces a surface charge distribution on the cell in the form of an electric dipole moment, whose magnitude and polarity depends on the frequency-dependent dielectric polarizabilities of the cell and surrounding medium [4]. If the field is non-uniform (i.e., there is a local field gradient) a DEP force will act on the induced dipole moment, causing a freely suspended cell to move. An example of the modeling of the vector dot-product $(E.\nabla)E$ of the field and field gradient in the neighbourhood of an ITO-hole is shown in Fig.2, along with a schematic to show how cells experiencing negative DEP are directed away from the edge of a hole and corralled together into a multi-cell construct. The electric field modeling was performed using FEMLAB software (COMSOL Multiphysics version 3.2). This modeling demonstrated (for a fixed concentration of cells in the initial suspension) that the overall size, shape and cell density of the cell construct shown in Fig.2 is determined by the diameter and relative locations of the ITO-holes, the thickness of the ITO layer on the

upper glass substrate, and by the distance between the top and bottom ITO electrodes. The choices of the various dimensions used in the DEP chamber and micromachining of the ITO electrodes were directed by our objective to engineer cell aggregations that mimic the dimensions of islets of Langerhans and are arrayed in rough correspondence to a 1536 microtitre plate format.

3. Results

The mean values obtained for the cell radius r, and the frequency f_{pk} at which the anti-field electrorotation rate was a maximum, are shown in Table 1 and Fig.3. The straight lines and formulae shown in Fig.3 are the best linear regression plots obtained using the Microsoft Excel program. The average radius of the INS-1 cells (n = 91) was determined to be 5.28 (± 0.69) microns, and 5.07 (± 0.64) microns for the BTC-6 cells (n = 97).

Based on the relevant theory and our experimental conditions [20], a plot of $f_{pk}.r$ against solution conductivity should be linear (of the form y = mx + c) and of slope m given by

$$m = \frac{1}{\pi C_m} \tag{1}$$

with an intercept c given by

$$c = \frac{m\, r\, G_m}{2} \tag{2}$$

In these equations C_m is the capacitance per unit area of the cell membrane, and G_m is the total effective membrane conductance. This total conductance comprises contributions arising from the passive conduction of ions on the surface and across the membrane [20].

From (1), with slope values *m* of 26 and 22 $m^2S^{-1}s^{-1}$ given in Fig.3, membrane capacitance values of 12.2 and 14.5 mFm^{-2} are derived for the INS-1 and BETA-TC-6 cells, respectively. This result for the INS-1 cells falls at the upper end of the range of values of 10.65 (± 2.1) and 10.23 (± 2.1) mFm^{-2} obtained in previous electrorotation studies [20]. Membrane capacitance values correlate closely with the extent to which the area of an otherwise smooth membrane surface is increased as a result of the presence of membrane folds and proturbances, such as blebs and microvilli [21, 22]. The larger capacitance values obtained in this present work can therefore be interpreted as the cells having a more complex surface morphology. This possibly reflects that the cells used in the previous work [20] were harvested from a relatively old culture (number of passages greater than 20), whereas the cells used in this present study were obtained from passages 5-7 of a fresh culture. Repeated passaging of insulin secreting cells is known to correlate with a loss of vesicle fusion [23]. This would be expected to correspond with a less 'detailed' membrane surface. The BETA-TC-6 cells used in these studies appear to exhibit a more complex membrane surface morphology than the INS-1 cells. Based on the intercept values of 0.023 and 0.015 ms^{-1} given in Fig.3, together with the average radius values of 5.28 (± 0.69) and 5.07 (± 0.64) μm, from (2) values for the total effective membrane conductance of 340 (± 45) and 274 (± 35) Sm^{-2} are obtained for the INS-1 and BETA-TC-6 cells, respectively. The conductance values observed for the INS-1 cells overlaps that of 261 (± 85) Sm^{-2} obtained previously for this cell type [20]. From this data the DEP responses expected for the INS-1 and BETA-TC-6 cells can be derived, based on the *smeared-out sphere* model to describe the dielectric polarizability of a cell [24]. Examples of this are shown in Fig.4 to cover the full range, 10-120 mS/m, of the suspending medium conductivity used in our studies.

The results shown in Fig.4 indicate that for an electric field frequency of 10kHz, using isotonic suspending media conductivities of 25~75 mS/m, the INS-1 and BETA-TC-6 cells should be repelled from the ITO-holes by negative DEP. At frequencies around 100kHz the cells should experience a weak or no DEP force, whilst for frequencies around 1-10MHz they should be attracted to the edges of the ITO-holes by positive DEP. Examples of this behavior are shown in Figs.5&6. In Fig.5, the action of a 10kHz, 4Vpk-pk, signal applied to cells suspended in a medium of conductivity 54.7 mS/m is shown to result in the cells being repelled from the ITO-hole edges, either into the bulk fluid between the holes or, more importantly for our purposes, into densely packed cell aggregations within the bulk fluid regions defined by the perimeters of the ITO-holes. In Fig.6, two sets of images provide evidence that the simple ITO-hole geometry can be used to manipulate cells located within the perimeters of the holes by both positive and negative DEP. The ability to push cells together and then pull them apart, repeatedly if desired, had previously been demonstrated using quadrupole electrodes [24], but the effect shown in Fig.6 of cells being extracted from other cells was not expected. This result indicates that the simple ITO-hole geometry might also provide the means to selectively sort cells, according to their dielectric phenotype, before they are directed into cell aggregations.

It was found experimentally that the excess cells, distributed in the bulk fluid between the ITO-holes, could be removed by flowing fluid through the DEP chamber whilst maintaining the integrity of the cell assemblies. With the negative DEP force in operation, the cell aggregations remained in place, even under conditions of high fluid flow rates (>50 ml/s) and mechanical agitation (including accidental dropping!) of the DEP chamber.

However, as shown in Fig.7, the cell aggregations did not survive the effect of a passing fluid-air meniscus. These results suggest that it would be possible to pass a gel forming solution through the DEP chamber, so as to encapsulate the cell aggregations in, for example, a porous

organosilicon matrix that permits the passage of nutrients and by-products to and from the cells.

Experiments were also performed to demonstrate that fluorescent PEBBLE nanosensors could be embedded into the cell assemblies, and used as real-time monitors of such parameters as pH and dissolved oxygen levels. The nanosensor particles were mixed with the cells prior to their admission into the DEP chamber. Fig.8 shows images, obtained using a Zeiss LSM-510, multiphoton confocal microscope, taken at a plane 60 μm below the top of a cell+PEBBLE assembly. These images demonstrate that the PEBBLE nanosensors were distributed throughout the cell aggregations. Furthermore, confocal microscopic examinations have shown that some aggregations were approximately 150 μm in diameter, 120 μm in height, and contained around 1000 cells. It is therefore possible to produce artificial cell constructs of the same size and cell density as a typical islet of Langerhans.

4. Conclusions

The DEP chamber used in these experiments consisted of a very simple geometry, namely that of a capacitor formed by two parallel glass slides of 220 μm separation, each coated with conducting indium tin oxide (ITO). The ITO coatings were ~110 nm thick, and thus transparent. The uniform electric field that would otherwise be produced between the two electrodes was disrupted by 100 holes machined into and through the top ITO coating. Each hole was of 200 μm diameter and spaced 600 μm apart as a 10x10 array. The footprint of this array is compatible with that of a 1536 microtitre plate, and thus potentially amenable to optical interrogation using automated plate-reading equipment. This was an important consideration because of our long-term objective to use fluorescent nanosensors to monitor cell physiological activities in real-time.

The decision to machine holes of roughly the same diameter as the electrode separation (~220 μm) was aided by theoretical modeling of the electric field distortion (calculated as the product of local field strength and field gradient) created by their presence in one of the electrode planes. The negative DEP forces generated by this field non-uniformity was found to be sufficiently strong to condense suspensions of BETA-TC-6 and INS-1 cells into three-dimensional cell constructs of roughly the same size and cell density as the pancreatic structures, known as islet of Langerhans, that regulate insulin levels in the blood. These constructs formed under the upper slide, where the ITO holes had been machined away, and protruded down into the perfusate. Furthermore, with the DEP force maintained, these three-dimensional multicell constructs were found to be robust enough to withstand mechanical shock and fluid flow forces. This could permit their encapsulation using a gel forming solution. Another important finding was that fluorescent PEBBLE nanosensors, which we plan to use as non-intrusive, real-time, probes of extracellular key biological species, can readily be incorporated into these artificial cell constructs.

The simple electrode geometry described here was also found to permit controlled manipulation of the cells by both positive and negative DEP, and the ability to achieve this was aided by acquisition of the dielectric properties of the cells, in terms of their membrane capacitance and conductance, by means of electrorotation measurements.

Taken together, the results of this and the previous study [20] provide a new methodology for addressing questions related to cell-cell communication, vesicle fusion and insulin release. Using the DEP formation of pseudo-islets of Langerhans we will be able to explore the nature and time scale of junctional complex formation, particularly gap junctions, and their role in

islet activity coordination. The ability to co-localize the PEBBLEs within the cell aggregates also advances a novel method to observe changes in the extracellular activity of metabolites or ions during physiological responses.

5. Acknowledgements

This study was financed by NIH grants NCRR RR001395 and DK06984 to P.J.S. Smith, the Alix and Denis Robinson Fund, and by the award to R. Pethig of the Eugene and Millicent Bell Tissue Engineering Fellowship at the MBL, Woods Hole. The authors thank Leon Collis, Mike Dacey and James Pringle for their assistance, and Tamara Clark for her artwork.

6. References:

1. Porterfield, D.M., Corkey, R.F., Sanger, R.H., Tornheim, K., Smith, P.J.S., and Corkey, B.E.: 'Oxygen consumption oscillates in single clonal pancreatic β-cells (HIT)', *Diabetes*, 2000, **49**, pp.1511-1516

2. Jung, S.K., Trimarchi, J.R., Sanger, R.H., and Smith, P.J.S.: 'Development and application of a self-referencing glucose microsensor for the measurement of glucose consumption by pancreatic β-cells', *Anal. Chem.*, 2001, **73**, pp.3759-3767

3. Smith, P.J.S. and Trimarchi, J.R.: 'Noninvasive measurement of hydrogen and potassium ion flux from single cells and epithelial structures', *Am. J. Physiol*., 2001, **280**, pp.C1-C11

4. Pethig, R.: 'Dielectrophoresis of Biological Cells', *Encyclopedia of Surface and Colloidal Science, 2nd Edition*, Taylor & Francis, New York, 2006, pp.1719-1736

5. Bertram, R., Previte, J., Sherman, A., Kinard, T.A., and Satin, L.S.: 'The phantom burster model for pancreatic beta-cells', *Biophys. J*., 2000, **79,** pp. 2880-2892

6. Bertram, R., and Sherman, A.: 'Dynamic complexity and temporal plasticity in pancreatic □-cells', *J. Biosci*., 2000, **25**, pp. 197-209

7. Balda, M. S., and Matter, K.: 'Epithelial cell adhesion and the regulation of gene expression', *Trends Cell Biol.*, 2003, **13**, pp.310–318

8. Zamir, E., Katz, B.Z., Aota, S., Yamada, K.M., Geiger, B., and Kam, Z.: 'Molecular diversity of cell-matrix adhesions**'** *J. Cell. Sci*., 1999, **112 (11)**, 1655-1669

9. Mueller-Klieser, W.: 'Three-dimensional cell cultures: from molecular mechanisms to clinical applications'**,** *Am. J. Physiol***,** 1997**, 273 (4)**, pp.C1109-C1123

10. Weaver, V.M., Lelievre, S., Lakins, J.N., Chrenek, M,A,, Jones, J.C.R., Giancotti, F., Werb, Z., and Bissell, M.J.: 'Beta 4 integrin-dependent formation of polarized three-dimensional architecture confers resistance to apoptosis in normal and malignant mammary epithelium', *Cancer Cell*, 2002, **2 (3)**, pp.205-216

11. Uroukov, I.S., Ma, M., Bull, L., and Purcell, W.M.: 'Electrophysiological measurements in three-dimensional in vivo-mimetic organotypic cell cultures: Preliminary studies with hen embryo brain spheroids', *Neurosci. Lett.*, 2006, **404**, pp.33-38

12. Suehiro, J., and Pethig, R.: 'The dielectrophoretic movement and positioning of a biological cell using a three-dimensional grid electrode system', *J. Phys. D: Appl. Phys.*, 1998, **31**, pp. 3298-3305

13. Flores-Rodriguez, N., and Markx, G.H.: 'Flow-through devices for the AC electrokinetic construction of microstructured materials', *J. Micromech. Microeng.*, 2006, **16**, 349-391

14. Sebastian, A., Buckle, A-M., and Markx, G.H.: 'Formation of multilayer aggregates of mammalian cells by dielectrophoresis', *J. Micromech. Microeng.*, 2006, **16**, 1769-1777

15. Albrecht, D.R., Underhill, G.H., Wassermann, T.B., Sah, R.L., and Bhatia, S.N.: 'Probing the role of multicellular organization in three-dimensional microenvironments' *Nature Methods*, 2006, **3 (5)**, pp.369-375

16. Burt, J.P.H., Goater, A.D., Menachery, A., Pethig, R., and Rizvi, N.H.: 'Development of microtitre plates for electrokinetic assays', *J. Micromech. Microeng.*, 2007, **17**, pp. 250-257

17. Brasuel, M., Kopelman, R., Aylott, J.W., Clark, H., Xu, H., Hoyer, M., Miller, T.J., Tjalkens, R., and Philbert, M.A.: 'Production, characteristics and applications of fluorescent PEBBLE nanosensors: Potassium, oxygen, calcium and pH imaging inside live cells', *Sensors & Materials*, 2002, **14 (6)**, pp. 309-338

18. Koo, Y.L., Cao, Y., Kopelman, R., Koo, S.M., Brasuel, M., and Philbert, M.A.: 'Real-time measurements of dissolved oxygen inside living cells by organically modified silicate fluorescent nanosensors', *Anal. Chem.*, 2004, **76 (9)**, pp. 2498-2505

19. Farfari, S., Schultz, V., Corkey, B.E., and Prentki, M.: 'Glucose-regulated anaplerosis and cataplerosis in pancreatic β-cells', *Diabetes* 2000, **49**, pp. 718-726

20. Pethig, R., Jakubek, L., Sanger, R.H., Heart, E., Corson, E., and Smith, P.J.S.: 'Electrokinetic measurements of membrane capacitance and conductance for pancreatic β-cells', *IEE. Proc.-Nanobiotechnol.*, 2005, **152**, pp. 189-193

21. Rothschild, Lord: 'The membrane capacitance of the sea urchin egg', *J. Biophysic. Biochem. Cytol.*, 1957, **3(1)**, pp. 103-111

22. Sukhorukov, V.L., Arnold, W.M., and Zimmermann, U., Hypotonically induced changes in the plasma membrane of cultured mammalian cells', *J. Membrane Biol.,* 1993, **142**, pp. 27-40

23. Zhang, H.J., Walseth, T.F., and Robertson, R.P.: 'Insulin secretion and cAMP metabolism in HIT cells: Reciprocal and serial passage-dependent relationships', *Diabetes*, 1989, **38**, pp. 44-48

24. Huang, Y., Hölzel, R., Pethig, R., and Wang, X.B.: 'Differences in the AC electrodynamics of viable and non-viable yeast cells determined through combined dielectrophoresis and electrorotation studies', *Phys. Med. Biol*., 1992, **37 (7)**, pp. 1499-1517

Table 1: Values of the radius r, and the frequency f_{pk} defining the maximum anti-field electrorotation rate, obtained for BTC-6 and INS-1 cells. Mean and standard deviation values are given for r and the product $f_{pk}.r$ for cells (number n) suspended in media of different conductivities.

Conductivity, mSm^{-1}	Cells, n	Radius r, μm	$f_{pk}.r$ ms^{-1}
BTC-6			
11.8	29	5.2 (0.57)	0.26 (0.09)
54.7	35	5.3 (0.66)	1.26 (0.27)
103.6	33	4.9 (0.64)	2.30 (0.33)
INS-1			
11.8	30	5.3 (0.72)	0.35 (0.08)
54.7	31	5.1 (0.71)	1.42 (0.22)
103.6	30	5.3 (0.61)	2.75 (0.33)

Figure Legends

Fig.1: The DEP chamber (left) consisted of two ITO-coated microscope slides, spaced 220 μm apart, encased in poly-dimethylsiloxane (PDMS). 1 mm diameter holes were drilled into the top wall and were used as fluidic ports. (Right) Four of the 10x10 array of 200μm diameter holes laser machined into the ITO layer of the top electrode. As a result of an optical artifact, the holes appear as annular rings.

Fig.2: (Left) Computerized plot of the scalar magnitude of the product of the field and field gradient ([E.∇]E) in the region of an ITO-hole. The largest value (~$3x10^{16}$ V^2m^{-3}) shown here occurs immediately below the edges of a 200μm diameter ITO-hole. A cell experiencing negative DEP will be directed away from such large ([E.∇]E) values (red colour) towards regions where the field is more uniform (purple colour). (Right) Schematic of cells directed by a negative DEP force to form an aggregate of cells. Other cells are pushed away into the bulk perfusate.

Fig.3: Plots of the electrorotation data given in Table 1 for the INS-1 and BETA-TC-6 cells. The straight lines represent the best linear regression plots of the data, and the corresponding linear equations are presented. Standard deviation values for the data points are given in Table 1.

Fig.4: The dielectrophoretic responses derived for INS-1 cells (solid-lines) and BETA-TC-6 cells (dotted-lines), for two conductivity values of the suspending medium, using the *smeared-out sphere* model of a cell [22]. Parameters used in this model included: radii values of 5.28 and 5.07 μm; membrane capacitances of 12.2 and 14.5 mFm^{-2}; membrane conductances of 340 and 274 Sm^{-2}, derived for the INS-1 and BETA-TC-6 cells, respectively.

Fig.5: (Left) An image, taken through the top of the DEP chamber, of INS-1 cells (~$5x10^6$ cells/ml) directed by negative DEP away from the edges of four ITO-holes into the bulk perfusate, either outside or within the hole perimeter boundaries. (Right) BETA-TC-6 cells (~10^8 cells/ml) directed by negative DEP into a densely packed assembly beneath a hole perimeter. Confocal microscopy revealed that this aggregate was ~ 75μm in height,

corresponding to 7~8 stacked layers of cells. For each image the conductivity of the suspending medium was 54.7 mSm^{-1}, and a 10kHz, 4V pk-pk, signal was applied.

Fig.6: Sequence of timed images of INS-1 cells (~$2x10^6$ cells/ml) being attracted (top row) to an ITO-hole edge by positive-DEP using a 15MHz, 4V pk-pk, signal. On changing the signal frequency from 15MHz to 1kHz, the cells are then pushed away (bottom row) from the perimeter by negative-DEP. Two cells (arrowed) have escaped from the ITO-hole perimeter into the surrounding bulk fluid.

Fig.7: Images taken as the bulk fluid is removed from the DEP chamber at a fluid rate ~25ml/s, whilst maintaining a negative DEP force generated by a 10kHz, 4V pk-pk, signal. BETA-TC-6 cells held beneath the ITO-holes by negative DEP remained in place, whereas other cells were removed. As expected, the DEP-induced cell constructs were dislodged (lower left) as a fluid-air meniscus advanced (from right to left) past them.

Fig.8: Confocal microscope images, taken at a plane 60 μm below the top of an assembly of INS-1 cells and embedded PEBBLE nanosensors, in a medium containing 10 mM glucose and of conductivity 51.5 mSm^{-1}. Confocal microscopy revealed that this assembly was approximately 150 μm in diameter, 120 μm in height, and contained around 1000 cells. The centre and right-hand images show preliminary measurements exploiting green and red fluorescent PEBBLEs to probe pH and oxygen levels, respectively.

Figure 1

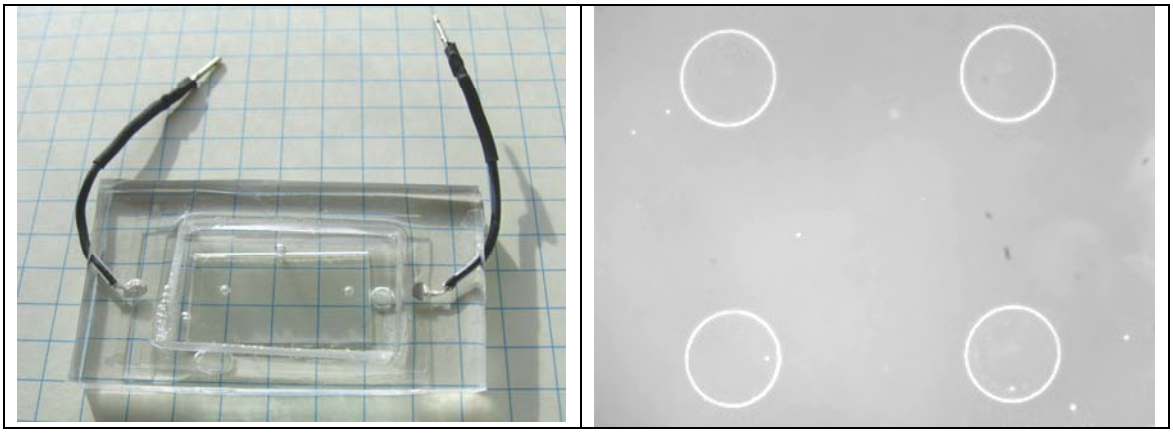

Figure 2

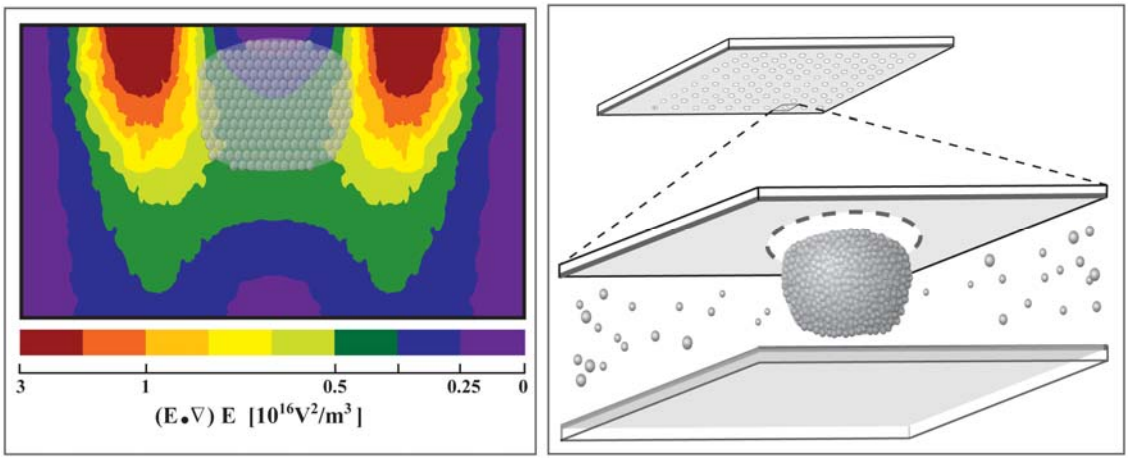

Figure 3

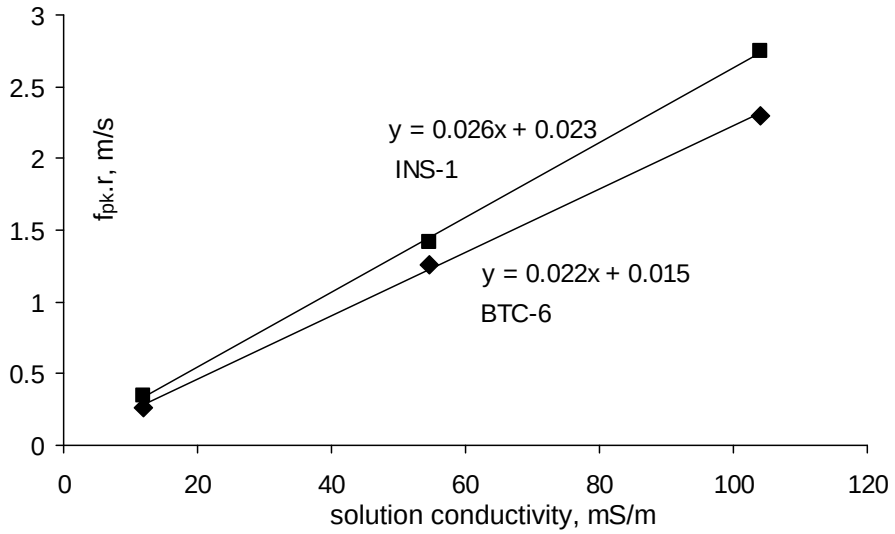
3
2.5
2
1.5
1
0.5
0
0
20
40
60
80
100
120
$f_{pk}.r$, m/s
solution conductivity, mS/m
y = 0.026x + 0.023
INS-1
y = 0.022x + 0.015
BTC-6

Figure 4

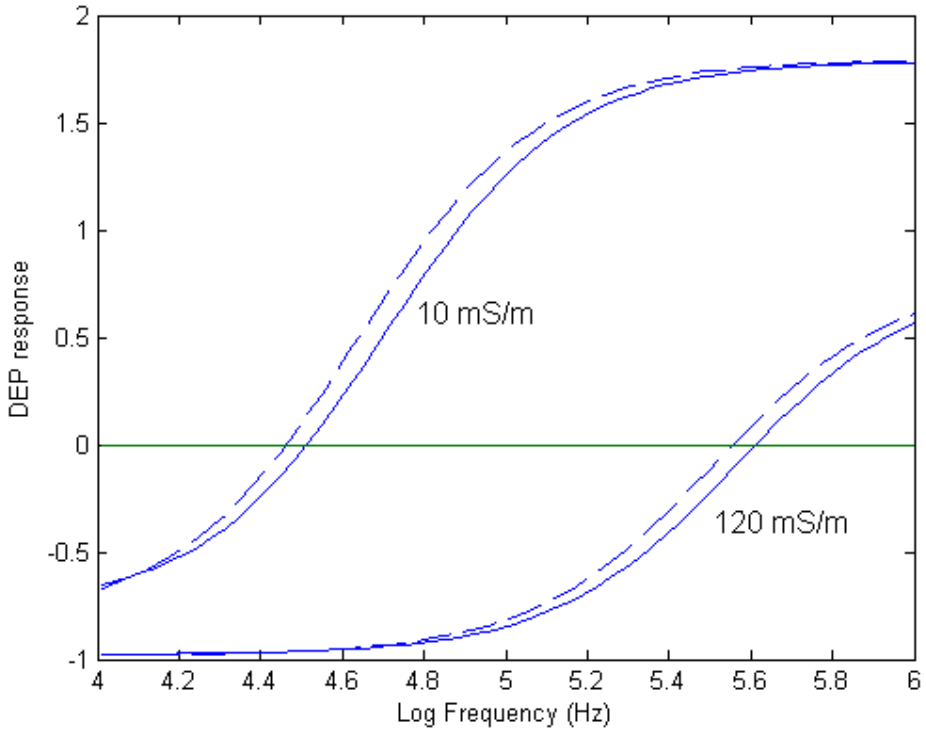
DEP response
Log Frequency (Hz)
10 mS/m
120 mS/m
2
1.5
1
0.5
0
-0.5
-1
4
4.2
4.4
4.6
4.8
5
5.2
5.4
5.6
5.8
6

Figure 5

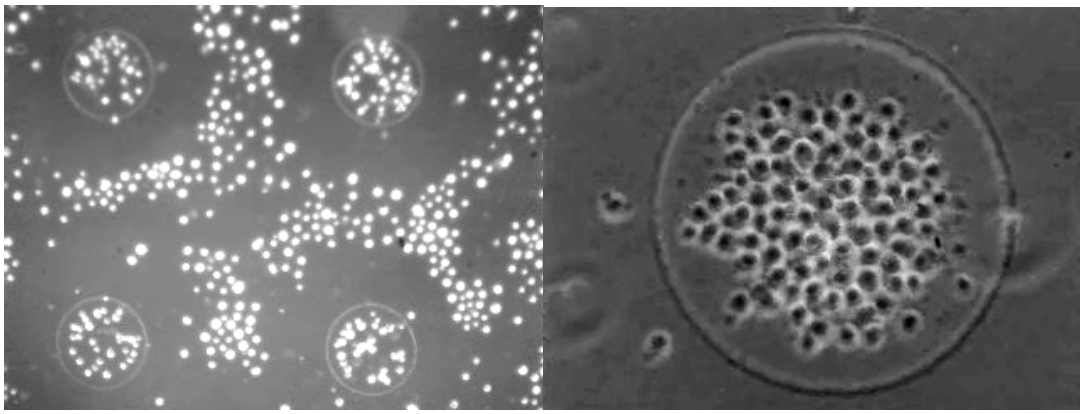

Figure 6

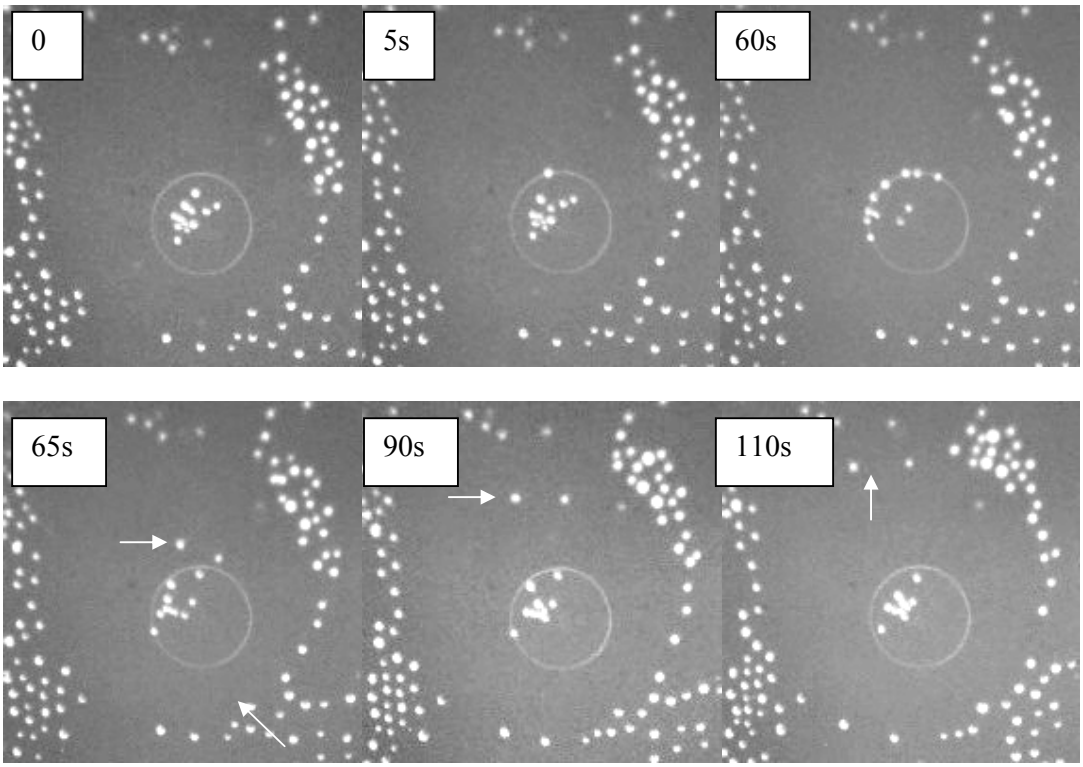

Figure 7

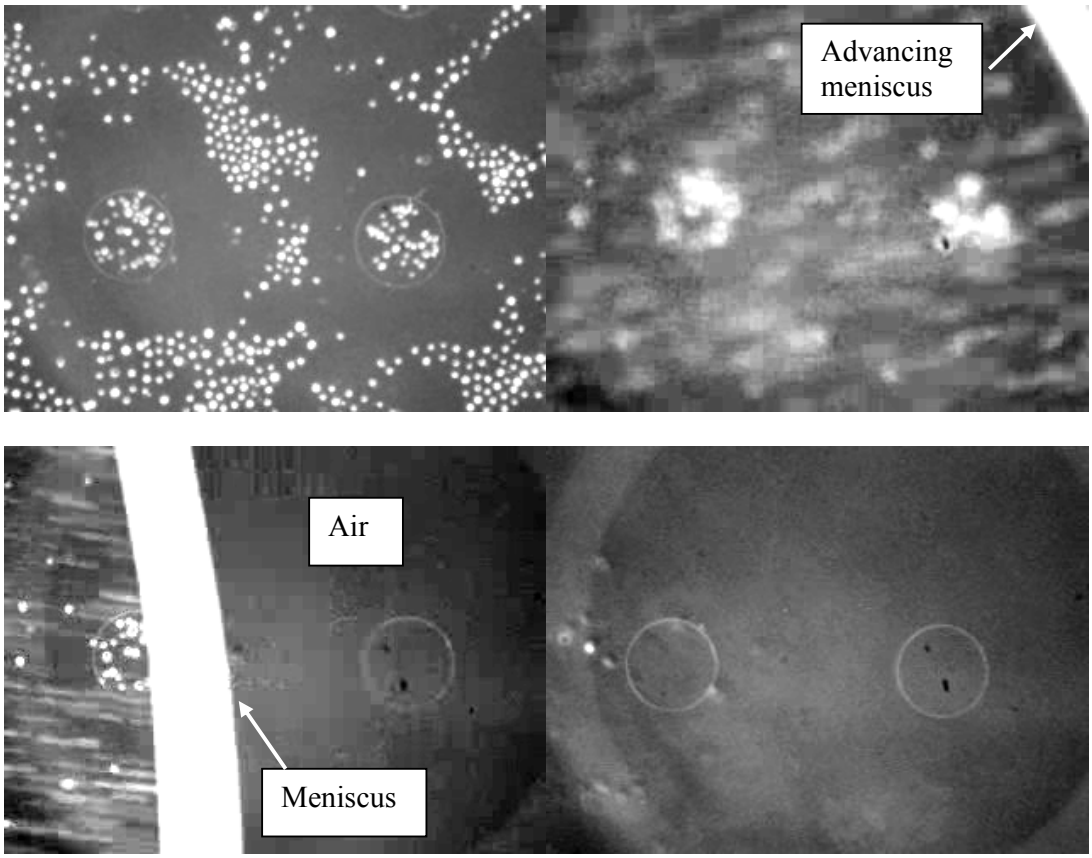

Figure 8